Control No. AP264

EFFECTS OF BOTTOM SLIP AND VARIABLE EDDY VISCOSITY IN HYDRODYNAMIC MODELS OF LAKE ST CLAIR

by

T.J. Simons and W.M. Schertzer

National Water Research Institute

Canada Centre for Inland Waters

Burlington, Ontario, Canada L7R 4A6

January 1987

NWRI Contribution #86-209

MANAGEMENT PERSPECTIVE

Knowledge of water movements is a prerequisite to understanding water quality properties of large lakes. Aquatic biologists and chemists, trained to deal with characteristic dimensions of a fish tank and accustomed to applying the same methodologies to laboratories, ponds, small lakes and inland seas, are beginning to realize that a water sample at a given time and location in a large water basin must be compared with an earlier sample from the same water mass rather than the same location. State-of-the-art water quality models of large lakes incorporate water exchanges between individual compartments as a matter of course, in particular near the shores where wind-driven water displacements are often reminiscent of river flows. Increased concern with contaminant exchanges at the sediment-water interface has added a new dimension to the problem of water movements. It is no longer sufficient to know the mass transport integrated over a water column but it has become necessary to evaluate the vertical structure of the flow and, especially, the current near the bottom. This problem is addressed in the present study.

An earlier report by the same authors was devoted to the design of a hydrodynamical model suitable for modelling material transport in Lake St. Clair. Results of the model were compared with extensive current meter observations during 1985 as part of the 1985/87 Canada-U.S. Upper Great Lakes Connecting Channel Study. The report

provides a very simple and economical procedure for computing water circulations in Lake St. Clair as required for many practical applications. However, a shortcoming of the model is its tendency to underestimate currents near the bottom. This property of the model is associated with assumptions concerning the vertical distribution of turbulent mixing which are mathematically convenient but physically unrealistic. The present report discusses two alternatives to remedy this problem.

While the models described in this report are much more flexible and more easily adaptable to measured current profiles, these advantages are achieved at the expense of added computational effort. However, experiments with these models show that the increased effort is a small price to pay for the resulting benefits when dealing with practical situations involving the movement of water near the bottom of a lake. In addition, the continuing rapid development of electronic computers renders the question of computing time increasingly irrelevant.

ABSTRACT

Two modifications of the conventional steady-state Ekman model with constant eddy viscosity and zero bottom velocity are considered. In the first case the constant eddy viscosity is retained but the no-slip bottom condition is replaced by a quadratic relationship between bottom stress and bottom current. In the second case the constant eddy viscosity is replaced by an arbitrary vertical profile of eddy viscosity and high-resolution finite-difference methods are employed to solve the vertical Ekman problem. Both methods are applied to Lake St. Clair and the results are compared with current measurements made during 1985 and with results from the basic model with constant eddy viscosity and zero bottom slip. It is shown that the modified models remedy the major shortcoming of the basic model which underestimates current speeds near the bottom.

PERSPECTIVE ADMINISTRATIVE

Il est essentiel de connaître les déplacements des eaux pour comprendre les caractéristiques qualitatives des eaux des grands lacs. Les biologistes et les chimistes aquatiques, habitués à mesurer leurs paramètres dans des bassins aux dimensions d'un aquarium et à appliquer les mêmes méthodes en laboratoire, dans les étangs, les petits lacs et les mers intérieures, commencent à se rendre compte qu'un échantillon d'eau prélevé à un moment donné dans un endroit donné dans un grand bassin hydrogrpahique doit être comparé à un échantillon angérieur provenant de la même masse d'eau plutôt que du mme endroit. Les modèles les plus récents de la qualité de l'eau des grands lacs tiennent compte des echanges d'eau entre les compartiments individuels, et notamment près des berges où les déplacements d'eau provoqués par le vent ressemblent souvent à l'écoulement en rivière. L'attention que l'onporte de plus en plus aux échanges de contaminants à l'interface sédiments-eau a ajouté une nouvelle dimension au problème du déplacement des eaux. Il ne suffit plus aujour'hui de connaître le transport de masse intégré dans une colonne d'eau; il est devenu nécessaire d'évaluer la structure verticale de l'écoulement et, notamment, le courant près du fond. C'est sur ce problème que s'est penchée la présente étude.

Un rapport antérieur des mêmes auteurs était consacré à la conception d'un modèle hydrodynamique qui convienne à la modélisation du transport des matériaux dans le lac Saint-Claire. Les résultats

obtenus ont été comparés aux observations exhaustives au courantomètre effectuées en 1985 dans le cadre de l'étude Canada-Etats-Unis sur les canaux reliant les Grands Lacs d'amont de 1985/1987. Le rapport donne une méthode très simple et très économique répondant à de nombreuses applications pratiques pour calculer la circulation de l'eau dans le lac Sainte-Claire. Toutefois, une des lacunes du modèle est de sourvent sous-estimer les courants près du fond. Cette lacune découle des hypothèses concernant la distribution verticale du brassage turbulent, hypothèses concernant la distribution verticale du brassage turbulent, hypothèses qui sont commodes du point de vue mathématiques, mais qui ne correspondent pas à la réalité. Le présent rapport étudie deux options pour corriger ce problème.

Bien que les modèles décrits dans ce rapport soient beaucoup plus souples et beaucoup plus facilement adaptables à des profils de courants mesurés, ils exigent cependant un effort de calcul supplémentaire. Toutefois, les expériences effectuées montrent que cet effort vaut la peine compte tenu des avantages de ces modèles pour l'analyse de situations pratiques mettant en jeu des déplacementd d'eau près du fond d'un lac. En outre, le développement rapide des ordinateurs électroniques rend le problème du temps de calcul de plus en plus insignifiant.

RÉSUMÉ

Deux modifications du modèle classique de régime permanent d'Ekman avec coefficient de frottement intérieur constant et vitesse d'écoulement de fond nulle sont envisagées. Dans le premier cas, le coefficient de frottement intérieur constant est retenu, mais les conditions de glissement de fond nul sont remplacées par un rapport quadratique entre la pression de fond et le courant de fond. Dans le second cas, le coefficient de frottement intérieur constant est remplacé par un profil vertical arbitraire de frottement intérieur et des méthodes aux différences finies à haute résolution sont utilisées pour résoudre le problème vertical d'Ekman. Les deux méthodes sont appliquées au lac Sainte-Claire et les résultats sont comparés aux mesures de courant effectuées en 1985 ainsi qu'aux résultats d'un modèle de base avec coefficient de frottement intérieur constant et glissement de fond nul. Il apparaît que les modèles modifiés corrigent la principale lacune du modèle de base qui sous-estime les vitesses du courant de fond.

1. INTRODUCTION

The overall objective of this investigation is to model material transport and sediment-water exchanges in Lake St. Clair as part of the 1985/87 Canada-U.S Upper Great Lakes Connecting Channel Study. The specific objective addressed in this report is development of a hydrodynamic model suitable for simulating water movements in Lake St. Clair and verification of this model against extensive current meter observations carried out during 1985. In an earlier report on this subject (Simons and Schertzer, 1986), it was shown that the circulation in Lake St. Clair adjusts itself rapidly to changes in wind forcing and that within a few hours a quasi-steady balance is achieved between wind and currents. Since the time scales of pollutant transport problems are typically in the range of days to years, it was concluded that an appropriate circulation model should be based on the theory of three-dimensional steady-state currents induced by winds. The response of the lake to wind then consists of a gradual transition from one steady-state solution to the next.

Conventional solutions for three-dimensional distributions of steady-state currents in homogeneous water are based on Ekman theory with constant eddy viscosity and zero bottom velocity. This type of Ekman model was used in the earlier work cited above. While the model produced generally adequate simulations of observed currents, it was found that the current speeds near the bottom were severely

underestimated. It was noted that this was to be expected from an Ekman model with a no-slip boundary condition at the bottom of the lake in conjunction with the constant eddy viscosity. The purpose of the present study is to remedy these shortcomings so as to obtain a more realistic vertical profile of the current near the bottom. The model results will then be compared with the available current measurements following the same procedures used in the earlier study.

It is known that the mathematically-simple Ekman model with constant eddy viscosity and zero bottom velocity is physically unrealistic. Near the bottom the eddy viscosity must decrease rapidly to a value close to zero and the Ekman layer changes into a logarithmic boundary layer. To deal with this problem, solutions have been proposed for various depth-dependent forms of the vertical eddy viscosity. A summary of earlier work may be found in Defant (1961) while some recent examples have been reported by Thomas (1975), Witten and Thomas (1976), Lai and Rao (1976) and Madsen (1977). An alternate procedure is to retain the constant eddy viscosity but replace the no-slip bottom condition by a more general statement relating bottom stress to bottom velocity (Nomitsu and Takegami, 1934; Birchfield, 1967; Jelesnianski, 1967; Heaps, 1972). Both of these approaches to the Ekman problem will be considered.

With regard to a more general bottom boundary condition, the simplest and most common procedure is to assume that the stress is parallel and linearly proportional to the velocity of the bottom

current. A shortcoming of this formulation is that the bottom stress is more likely a quadratic function of the bottom current and, hence, if a linearized stress formula is used, the coefficient itself should vary with the bottom current. Since this current may vary over a wide range, one has to deal with a new model parameter which is essentially unknown. Thus, the Ekman solution with generalized bottom slip but linearized bottom stress involves two adjustable parameters, the vertical eddy viscosity and the coefficient of the linearized stress fomulation.

The physically more realistic formulation of bottom stress as a quadratic function of bottom current was used in the Ekman problem by Nomitsu and Takegami (1934). While this formulation requires some additional computational effort, it has the advantage that the value of the drag coefficient in a nonlinear stress law has been fairly well established. Consequently, this procedure does not introduce another unknown parameter into the Ekman problem and, for practical purposes, the only adjustable model parameter is the eddy viscosity. In view of this, it was decided to apply the model with nonlinear bottom stress to Lake St. Clair.

With regard to vertical variations of eddy viscosity, most solutions to be found in the literature were derived for specific vertical profiles of eddy viscosity which permit analytical solutions of the Ekman equations. Such solutions express the depth-dependent current and the vertically-integrated current in terms of

pressure gradient and surface wind. The advantage is that these functions, once derived, can be rapidly evaluated for given values of eddy viscosity and depth. The disadvantage is that the formulas are inflexible with regard to the vertical profile of eddy viscosity. The rapid developments in computer technology have greatly reduced the advantage of closed-form solutions. Thus, the vertical Ekman equations can now be solved by high-resolution finite-difference methods without adding greatly to the time required for solving the three-dimensional steady-state circulation problem. This technique allows for an arbitrary vertical profile of eddy viscosity and will also be applied to Lake St. Clair in this study.

2. NONLINEAR BOTTOM STRESS

The usual procedure to solve the Ekman problem is to define the complex velocity

$$w = u + iv \tag{1}$$

The steady-state equation of motion then becomes

$$\frac{\partial^2 w}{\partial z^2} - \alpha^2 w = - \alpha^2 w_g \tag{2}$$

with

$$\alpha \equiv \frac{1+i}{\Delta} \qquad \Delta \equiv \sqrt{\frac{2\nu}{f}} \tag{3}$$

where z is the vertical coordinate, ν the constant kinematic eddy viscosity, f the Coriolis parameter, Δ the Ekman depth and w_g the constant geostrophic current with components

$$u_g = \frac{-1}{\rho f}\frac{\partial p}{\partial y} \qquad v_g = \frac{1}{\rho f}\frac{\partial p}{\partial x} \tag{4}$$

The boundary conditions are

$$\begin{aligned} \nu \frac{\partial w}{\partial z} &= \frac{\tau_s}{\rho} && \text{at} \quad z = 0 \\ w &= w_b && \text{at} \quad z = -h \end{aligned} \tag{5}$$

where h is the depth and τ_s the surface stress. In solving the Ekman problem, the pressure gradient (geostrophic current) and the surface stress are treated as known quantities. The solution is

$$w = w_b \frac{\cosh \alpha z}{\cosh \alpha h} + w_g \left(1 - \frac{\cosh \alpha z}{\cosh \alpha h}\right) + \frac{\tau_s}{\rho \nu \alpha} \frac{\sinh \alpha(h+z)}{\cosh \alpha h} \tag{6}$$

where the bottom current, w_b, still has to be determined. The solution (6) involves the same functions of the vertical coordinate as the conventional solution with zero bottom current. A review of these

functions may be found in Simons (1980, p. 36). For convenience, the formulas have been copied in the Appendix (Eqs. (3.6)-(3.8)).

The bottom stress is related to the bottom current by the quadratic relationship

$$\frac{\tau_b}{\rho} = c_D |w_b| \, w_b \tag{7}$$

The product $c_D|w_b|$ may be identified with the slip parameter of solutions with linearized bottom stress. Vertical integration of the original equation (2) and substituting (7) results into

$$c_D |w_b| w_b = - ifW + ifhw_g + \frac{\tau_s}{\rho} \tag{8}$$

The vertically-integrated current, W, follows from (6) and the result may be substituted into (8) in order to get an equation for the bottom current as a function of the pressure gradient and the surface stress

$$w_b \left[c_D |w_b| + \frac{\nu\alpha \sinh \alpha h}{\cosh \alpha h} \right] = w_g \frac{\nu\alpha \sinh \alpha h}{\cosh \alpha h} + \frac{\tau_s}{\rho} \frac{1}{\cosh \alpha h} \tag{9}$$

While this completes the formal solution of the Ekman problem, it remains to determine the pressure gradient or surface slope as a function of the horizontal coordinates for a basin subjected to wind forcing or affected by river flows. This is done by deriving the vorticity equation for the vertically-integrated current, W. The latter is found from (6) by substituting (8)

$$W(1+\delta) = w_g\left[h(1+\delta) - \frac{\sinh \alpha h}{\alpha \cosh \alpha h}\right] - \frac{i\tau_s}{f\rho}\left[1+\delta - \frac{1}{\cosh \alpha h}\right] \qquad (10)$$

where

$$\delta \equiv \frac{\nu\alpha}{c_D|w_b|}\frac{\sinh \alpha h}{\cosh \alpha h} \qquad (11)$$

For the basic solution with zero bottom current the bottom stress is non-zero and hence from (7) it follows that $c_D|w_b| \to \infty$ such that (11) gives $\delta \to 0$. Thus, the solution (10) involves the same depth-dependent coefficients as the basic solution. These coefficients may be found in Simons (1980, p. 37) and, in the same notation, (11) becomes $\delta=(A+iB)fh/c_D|w_b|$. Again, the formulas have been reproduced in the Appendix (Eqs. (3.10)-3.11)).

The vorticity equation is readily obtained by solving (10) for the geostrophic current in terms of the vertically-integrated current and the surface stress and cross-differentiating the two components of the geostrophic current (4). The result is, in form, identical to that for the conventional Ekman solution derived in Simons (1980, p. 74) and copied in the Appendix (Eqs. (5.14)-(5.16)) but the coefficients of the equation involve the parameter (11). (Note that the u-component of the current in the second of the two equations (5.14) in Simons (1980) has the wrong sign. This has been corrected in the equations reproduced in the Appendix.) The parameter (11) depends on the bottom velocity which can be found from (8) only after the vorticity equation has been solved for W and the geostrophic

current has been determined from (10). Therefore, the solution must be obtained by iteration on the bottom current. This iteration can be readily combined with the iteration required for solving the vorticity equation on a computational grid. A simple procedure is to start by solving the vorticity equation for W as in the conventional case with zero bottom current ($\delta=0$). Then the geostrophic current follows from (10), the bottom current from (8) or (9) and the new value of δ from (11). The corrected vorticity equation is then solved and the whole process is repeated. All experiments with the model applied to Lake St. Clair showed rapid convergence.

As compared to the more common procedure of assuming that the stress is linearly proportional to the current at the bottom (Jelesnianski, 1967; Birchfield, 1967) it is seen that the only additional effort is to compute the bottom velocity $|w_b|$ instead of assigning an arbitrary value to the slip parameter $C_D|w_b|$. This leads to the iteration procedure outlined above. It is, however, important to realize that the iteration is required to determine the magnitude or speed of the bottom current rather than the current vector. The appropriate equation follows from (8) or (9) by multiplication by the complex conjugate equation, thus obtaining an equation in which $|w_b|$ is the only unknown. Once this equation has been solved, the slip parameter is known and all equations are, in form, identical to those describing the Ekman problem with linear bottom slip.

3. ARBITRARY PROFILE OF EDDY VISCOSITY

If the eddy viscosity is a function of depth, the solution of equation (2) becomes rather complicated. For specific vertical variations of eddy viscosity, analytical solutions may be found in the literature. However, a solution which is completely flexible with regard to the eddy viscosity profile can be obtained only by finite-difference methods. A suitable procedure will be presented here. It will be assumed that the eddy viscosity becomes small near the bottom such that a no-slip bottom boundary condition can be applied.

Let the vertical water column of depth h be divided into N layers of depth $\Delta z=h/N$. Let the complex velocity defined in (1) be specified at the centre of each layer and the eddy viscosity, ν, at the interfaces between the layers. Replacement of vertical derivatives by central differences then leads to the set of steady-state equations

$$-\nu_{n-1}\, w_{n-1} + (\nu_{n-1} + \nu_n + if\Delta z^2)\, w_n - \nu_n\, w_{n+1} = if\Delta z^2 w_g \qquad (12)$$

The subscripts of the eddy viscosity range from 0 at the free surface to N at the bottom of the water column but the general form of (12) is valid only for n between 2 and N-1. For n =1, application of the upper boundary condition replaces the first two terms of (12) by

$$-\nu_0 w_0 + \nu_0 w_1 = -\Delta z \left(\nu \frac{\partial w}{\partial z}\right)_0 = -\Delta z \frac{\tau_s}{\rho} \qquad (13)$$

For n=N, the no-slip bottom boundary condition implies that $w_{N+1}+w_N=0$ and hence the last term on the left of (12) is replaced by

$$-\nu_N w_{N+1} = \nu_N w_N \tag{14}$$

The result is a system of N equations for the layer velocities w_n, n=1,2,...,N, which, in matrix notation, involves a tri-diagonal matrix of eddy viscosity values at various depths. This is a very common type of problem which can be solved rapidly by direct matrix inversion.

Like the conventional Ekman solutions, the current will be a function of the pressure gradient and the surface stress. In order to establish these functional relationships, equations (12)-(14) must be solved twice, once for the gradient current and once for the wind drift. In each case the two components of the current and the vertically-integrated current are obtained and, by comparison with the conventional Ekman solutions (see Appendix), the coefficients involved are determined.

The gradient current is computed for a unit geostrophic current $w_g=u_0=1.0$ m/s and zero surface stress. Using the notation of the Appendix and defining $\alpha'=\alpha/c$, $\beta'=\beta/c$, this current may be written

$$\frac{u}{u_0} = 1-\alpha'(z) \qquad \frac{v}{u_0} = \beta'(z) \qquad \frac{U}{u_0} = h\,(1-B) \qquad \frac{V}{u_0} = hA \tag{15}$$

and, hence, the numerical solution in this case essentially determines the coefficients α, β, A, B. Similarly, the wind drift is computed for a unit wind stress $\tau_s=\tau_0=1.0$ N/m^2 and zero geostrophic current. With the notation of the Appendix and defining $\gamma'=(\gamma+\varepsilon)\delta/c$ and $e'=(\varepsilon-\gamma)\delta/c$ this solution may be written

$$\frac{u}{\tau_0} = \frac{\gamma'(z)}{h\rho f} \qquad \frac{v}{\tau_0} = \frac{\varepsilon'(z)}{h\rho f} \qquad \frac{U}{\tau_0} = \frac{E}{\rho f} \qquad \frac{V}{\tau_0} = \frac{F-1}{\rho f} \tag{16}$$

which determines the coefficients γ, ε, E, F. Once the coefficients have been computed for all points of the horizontal grid, the solution of the vorticity equation proceeds in the same way as for the conventional Ekman solutions.

4. PROPERTIES OF SOLUTIONS

Results will be presented for the case of constant eddy viscosity with nonlinear bottom stress and for the case of vertical variation of eddy viscosity with zero bottom slip. These results will be compared with those obtained for constant eddy viscosity and zero bottom current in the earlier study by Simons and Schertzer (1986).

First, it is of interest to illustrate the general characteristics of the solutions, in particular the bottom stress and the current near the bottom. The water depth is assumed to be 5 m which is close to the average depth of Lake St. Clair. Examples will be presented of pressure-driven currents (such as the river-induced

flow through Lake St. Clair) and wind-driven currents. In the latter case it is assumed that the wind drift is balanced by return flow such that the total transport vanishes. This is the type of circulation encountered in a closed channel with constant depth. For nonlinear bottom stress, the return flow or geostrophic current follows from equation (10) for W=0. Since the solution depends on the bottom current which, in turn, depends on the geostrophic current by equation (8), iteration is required. As such, the method of solution is the same as for the two-dimensional model of Lake St. Clair.

In the case of constant eddy viscosity and nonlinear bottom stress, solutions will be compared for a drag coefficient, c_D, ranging from 10^{-3} to 10^{-2} and for zero bottom current. The latter is equivalent to $c_D \to \infty$ since the bottom stress (7) must be nonzero. In the case of variably eddy viscosity, numerical solutions are obtained by dividing the water column into 50 layers of depth 0.1 m each. The eddy viscosity selected for illustration has a linear profile with a bottom value equal to 10 percent of the surface value. The magnitude of the eddy viscosity in this case will be identified by the value at the free surface. Thus, for a given value, the vertical-mean eddy viscosity is about half as large as a vertically-uniform eddy viscosity with the same numerical value.

Figures 1 and 2 present results for pressure-driven currents. Figure 1 shows the bottom stress as a function of the geostrophic current and the eddy viscosity. Figure 2 shows the current at 1 m above the bottom in relation to the vertical mean current. The

current at 1 m above the bottom has been selected in view of the measurements at that level carried out in Lake St. Clair during 1985. In all illustrations, the curves labelled $v_b=0$ represent the conventional Ekman solution with constant eddy viscosity and zero bottom slip. As expected, the bottom stress reaches a maximum under these conditions. Since the vertical-mean value of the linear eddy viscosity is about one half of its surface value, the bottom stress for that case is comparable to one half of the bottom stress for constant eddy viscosity and no slip. As for the current at 1 m above the bottom, its amplitude is at least 80% of the vertical-mean current as compared to less than 60% for the conventional solution. The variation of current direction with depth is reduced considerably and hence the vertical profile of the current is much more uniform.

Figures 3 and 4 present results for wind-driven currents with total transport equal to zero. The nonlinear bottom stress decreases for increasing values of the eddy viscosity in contrast to the conventional case where the bottom stress approaches a value equal to 50 percent of the wind stress. Since the wind-induced water setup equals the net effect of surface and bottom stress, the setup is reduced substantially. The current at 1 m above the bottom is part of the return flow and therefore its speed increases by reduced bottom friction.

The properties of the solutions may be illustrated by considering small values of $|\alpha^2 h^2| = h^2 f/\nu$, i.e. shallow water or large eddy viscosity. Taking this limit of the general equation(10) one obtains

$$\bar{w}\left(1+i\frac{fh}{c_D|w_b|}\right) = \frac{h}{\rho\nu}\left[\tau_s\left(\frac{1}{2}+\varepsilon\right) - h\nabla p\left(\frac{1}{3}+\varepsilon\right)\right] \qquad \varepsilon \equiv \frac{\nu}{hc_D|w_b|} \tag{17}$$

where ∇p is the pressure gradient and $\bar{w}$ the vertical-mean current. Except for the second term on the left, this equation is the same as the solution for the case of no rotation. Since this term is independent of eddy viscosity, the present solution for large eddy viscosity does not become equivalent to the no-rotation solution and hence, in this regard, it differs from the conventional solution with zero slip. Similarly, equation (8) for the bottom current

$$c_D|w_b|w_b + ifh\bar{w} = \frac{\tau_s}{\rho} - \frac{h}{\rho}\nabla p \tag{18}$$

differs from the no-rotation case by the second term on the left. For the case of no bottom slip this term, by (17), is proportional to h^2f/ν and hence becomes negligible for small values of this parameter. Again, this is not necessarily so when bottom slip is included.

The pressure gradient is a function of the wind stress and the vertical-mean current which, in general, is non-zero and must be determined from the vorticity equation as outlined under Eq. (11). For a closed channel with uniform depth, however, the vertical-mean flow must vanish and hence the pressure gradient depends only on the wind stress. This dependence involves the parameter ε which, by (18), is a function of the pressure gradient itself. For large values of eddy viscosity the channel solution ($\bar{w}=0$) obtained from (17) is

$$h\nabla p = \tau_s \frac{1+1/2\varepsilon}{1+1/3\varepsilon} \approx \tau_s \left(1 + \frac{1}{6\varepsilon}\right) = \tau_s \left(1 + \frac{hc_D|w_b|}{6\nu}\right) \qquad (19)$$

When (19) is substituted into (18) the bottom current and bottom stress become

$$w_b \approx -\frac{h\tau_s}{6\nu\rho} \qquad \frac{\tau_s}{\rho} \approx -\frac{c_D h^2 |\tau_s| \tau_s}{36\nu^2\rho^2} \qquad (20)$$

In contrast to the case of no bottom slip where the bottom stress becomes one half of the wind stress for large eddy viscosity, the bottom stress decreases with increasing eddy viscosity in the present case. It also is proportional to the drag coefficient and the square of the wind stress. This explains the results of Figure 3. Note that corresponding relationships for a linear bottom stress formulation are obtained by replacing $c_D|w_b|$ by a constant slip parameter. The equation for the bottom current remains the same but the bottom stress becomes linearly dependent on wind stress and eddy viscosity.

3. APPLICATION TO LAKE ST. CLAIR

In the report by Simons and Schertzer (1986) a conventional Ekman model with constant eddy viscosity and no bottom slip was applied to Lake St. Clair and the results were compared with current measurements 1 m above the bottom carried out continuously between June 5 and November 5, 1985. The comparison concentrated on six current meters placed in a SW-NE transect of the lake (stations C1-C6 in Figure 5)

and the wind stress and currents were decomposed into components along the transect toward the NE (x-axis) and normal to the transect toward the NW (y-axis). Daily-averaged currents and winds were used and the model results were compared with an empirical model fitted to the measurements rather than with the measurements themselves. This condenses the comparison between data and model results into a few tables or diagrams. Two different comparisons were made. The first was based on the total transport of water through the transect C1-C6; the second dealt with currents at individual mooring stations.

For this study the vertically-integrated current was defined as the current at 1 m above the bottom multiplied by the depth. The corresponding water transport through the section was obtained by horizontal integration of the component normal to this section. The difference between this result and the true transport based on vertical-mean currents is a measure of the current profiles. Assuming linear dynamics the transport may be written

$$V = V_0 + \frac{\tau_x}{\tau_0} V_1 + \frac{\tau_y}{\tau_0} V_2 \qquad (21)$$

where V_0 refers to the hydraulic flow and V_1 and V_2 to the transports induced by a unit wind stress τ_0, in x- and y- direction, respectively. If τ_s is the magnitude of the stress and θ its direction clockwise from the x-axis, then the stress components are

$$\tau_x = \tau_s \cos\theta \qquad \tau_y = -\tau_s \sin\theta \qquad (22)$$

Substitution of (22) into (21) gives

$$\bar{V} = V_0 + \frac{\tau_s}{\tau_0} A \sin(\theta + \alpha) \qquad A = (V^2_1 + V^2_2)^{1/2} \qquad \tan\alpha = -V_1/V_2 \quad (23)$$

Given the series of daily-mean values of measured winds and water transports, the hydraulic and wind-driven components of the empirical model were determined by a least-squares fit. This was done for different classes of wind mixing as measured by the daily root-mean-square value of the stress. The results were compared with numerical model results for different values of eddy viscosity in order to estimate a relationship between eddy viscosity and wind mixing. Like the measured transport, the computed transport was based on the current computed at 1 m above the bottom and, hence, should not be identified with the true water transport through the section.

Table 1 compares the results from the empirical model with results of the conventional Ekman model with constant eddy viscosity and no slip and the two models presented in this report. As discussed by Simons and Schertzer (1986) the results suggest that the eddy viscosity in the conventional Ekman model should increase with wind mixing in approximately linear fashion. If the constant eddy viscosity is replaced by a linear variation of eddy viscosity with a bottom value equal to 10 percent of the surface value, the results are nearly the same if the eddy viscosity at the surface is about three times as large as the constant eddy viscosity. If the no-slip condition is replaced by a nonlinear bottom stress formulation with

c_D=.01, the value of the eddy viscosity must be increased again to offset the reduction in bottom stress (see Figs. 1 and 3). Since the latter model is nonlinear, the solution is not exactly a linear function of the wind stress as shown at the bottom of Table 1.

The linear model fitted to currents at individual mooring stations C1-C6 has the form

$$\begin{pmatrix} u \\ v \end{pmatrix} = \begin{pmatrix} u_0 \\ v_0 \end{pmatrix} + \begin{pmatrix} u_1 & u_2 \\ v_1 & v_2 \end{pmatrix} \begin{pmatrix} \tau_x/\tau_0 \\ \tau_y/\tau_0 \end{pmatrix} \qquad (24)$$

where the subscripts have the same meaning as in (21). In the empirical model, the elements of the hydraulic flow and the wind-response matrix were determined again by a least-squares fit to the measured currents. The numerical model results were obtained by forcing the model by river flows and wind stress components along (τ_x) and normal (τ_y) to the transect. The empirical results were obtained for different classes of the daily root-mean-square value of the wind stress; the hydrodynamic results were obtained for different values of eddy viscosity. The relationship between eddy viscosity and wind mixing follows then by matching the speeds and directions of the elementary currents (u_0,v_0), (u_1,v_1), (u_2,v_2) as obtained from the empirical and the numerical model, respectively. For a graphical comparison of the directions the reader is referred to Simons and Schertzer (1986). For the two models discussed in the present report, the results are similar but the analysis will concentrate on the current speeds which permit a more quantitative comparison.

Table 2 compares the speeds of the elementary currents averaged over the six stations C1-C6 at a level of 1 m above the bottom. The subscripts have the same meaning as in (21). The last column presents the average value of the current speeds induced by winds along and normal to the transect. It is seen that the speeds of wind-driven currents decrease with eddy viscosity in a similar way as with wind mixing and, hence, it follows that the vertical eddy viscosity is proportional to wind mixing. This is true for the modified Ekman models as well as for the basic model with constant eddy viscosity and without bottom slip. However, the numerical values of the eddy viscosity in the modified Ekman models must be increased to offset the reduction of bottom stress (see Figs. 1 and 3).

In the report by Simons and Schertzer (1986) it was noted that the main shortcoming of the Ekman model with constant eddy viscosity and without bottom slip was its tendency to underestimate current speeds near the bottom. In particular, the hydraulic currents computed by the numerical model were only half as large as those obtained from the empirical model. As expected, this error is substantially reduced in the model with linear eddy viscosity and even more so in the model with bottom slip. Both of these modifications result in lower bottom drag (see Fig. 1) and a more uniform vertical profile of the current (see Fig. 2).

The model with bottom slip is not exactly linear since the bottom stress is given by Eq. (7). The magnitude of the nonlinear effect is illustrated at the bottom of Table 2. Also, the hydraulic flow is not

completely uncoupled from the wind-driven flow. To evaluate this effect, calculations were made with a model forced by rivers and winds simultaneously, whereupon the hydraulic flow was subtracted to arrive at the wind-induced portion of the flow. These results differed by less than 10 percent from those presented in Table 2. Aside from the nonlinear effects, the model with bottom slip differs from those without slip in that the current speeds decrease much slower with increasing eddy viscosity. This may be explained by Eq. (17) which shows that the currents are inversely proportional to ν for the case of zero slip ($c_D|w_b| \to \infty$) but become independent of ν for large values of the parameter ε.

Another aspect of the solutions which deserves attention is the net effect of the bottom stress on the pressure gradient, i.e., the wind-induced water setup. For this purpose, model results were analyzed for a wind stress of 10^{-1} N/m^2 normal to the transect C1-C6. Since the mean depth of this transect is only 5.2 m the approximate equations (17) and (18) are valid for constant eddy viscosity with or without bottom slip. The solution for zero bottom slip has been discussed by Simons (1980, p. 76). In that case the setup $H\nabla p/\tau_s$ normal to the transect with mean depth H is greater than unity which implies that the net bottom stress makes a positive contribution to the setup. For the present model with nonlinear bottom stress and c_D=.01, the setup $H\nabla p/\tau_s$ normal to the transect was found to vary from 1.00 for ν=.0016 m^2/s to 0.93 for ν=.0048 m^2/s. Hence, the net contribution from the bottom stress to the setup is close to zero or negative.

From the same analysis of model results with bottom slip it was found that for $\tau_s=10^{-1}$ N/m^2 and $c_D=.01$ the bottom velocity averaged over the transect varied from 4.4 to 3.6 cm/s for ν varying from 16 to 48 x 10^{-4} m^2/s. This variation is much less than the one obtained from Eq. (20) for zero vertical-mean flow which would vary from 5.4 to 1.8 cm/s. Thus, for increasing values of eddy viscosity the solution with bottom slip becomes relatively insensitive to eddy viscosity, as seen already in Table 2.

As a final note it is interesting to compare the model with nonlinear bottom friction with a model with linear bottom friction applied to Lake St. Clair by Ibrahim and McCorquodale (1985). These authors calibrated their model by fitting computed currents to measurements made under relatively low wind speed conditions ($\tau_s \leq 0.05$ N/m^2). Their estimate of eddy viscosity was 20 x 10^{-4} m^2/s and the slip parameter equivalent to the product $c_D|w_b|$ was given as $0.3\ \nu/H \approx 1.2 \times 10^{-4}$ m/s. The present model with $c_D=.01$ and $\tau_s=.05$ N/m^2 gives typical bottom velocities of 2-3 cm/s for the same eddy viscosity which results in a slip parameter $c_D|w_b| \approx 2.5\times10^{-4}$ m/s, about twice as large as in the linear model. While this indicates a fair overall agreement between the two models, it must be realized that the bottom velocity in the model with nonlinear stress varies with water depth and wind stress as seen, for example, from Eq. (20).

REFERENCES

Birchfield, G.E., 1967: Horizontal transport in a rotating basin of parabolic depth profile. J. Geophys. Res., 72: 6155-6163.

Defant, A., 1961: Physical Oceanography. Pergamon Press, New York.

Heaps, N.S., 1972: On the numerical solution of the three-dimensional hydrodynamical equations for tides and storm surges. Mem. Soc. R. Sci. Liege, Ser. 6(2):143-180.

Ibrahim, K.A. and J.A. McCorquodale, 1985: Finite element circulation model for Lake St. Clair. J. Great Lakes Res., 11: 208-222.

Jelesnianski, C.P., 1967: Numerical computations of storm surges with bottom stress. Mon. Weather Rev., 95: 740-756.

Lai, R.Y.S and D.B. Rao, 1976: Wind drift currents in a deep sea with variable eddy viscosity. Arch. Meteor. Geophys. Bioklimatol., A25: 131-140.

Madsen, O.S., 1977: A realistic model of the wind-induced Ekman boundary layer. J. Phys. Oceanogr., 7: 248-255.

Nomitsu, T. and T. Takegami, 1934: Coast effect upon the ocean current and the sea level, I. Steady state. Mem. Coll. of Science, Kyoto Imperial Univ., Japan, Ser. A., 17: 93-141.

Simons, T.J., 1980: Circulation models of lakes and inland seas. Can. Bull. Fish. Aquat. Sci., 203, 146 pp.

Simons, T.J. and W.M. Schertzer, 1986: Hydrodynamic models of Lake St. Clair. NWRI Contribution #86-10, 54 pp.

Thomas, J.H., 1975: A theory of steady wind-driven currents in shallow water with variable eddy viscosity. J. Phys. Oceanogr., 5: 136-142.

Witten, A.J. and J.H. Thomas, 1976: Steady, wind-driven currents in a large lake with depth-dependent eddy viscosity. J. Phys. Oceanogr., 6: 85-92.

Table 1 Water transport across transect C1–C6 (Fig. 5) computed as NW component of current 1 m above the bottom multiplied by depth. Transport separated in hydraulic and wind-driven components as in Eq. (23) with unit wind stress $\tau_0 = 10^{-1}$ N/m^2 and angles clockwise from NE.

Empirical Model	$\hat{\tau}$ (10^{-2} N/m^2)		Transport (10^3 m^3/s)		
	Class	Mean	V_0	A	α
$\hat{\tau}$ = daily rms of wind stress	$\hat{\tau}<4.5$	2.8	-1.6	8.9	30
	$4.5<\hat{\tau}<9.0$	6.1	- .8	3.8	3
	$9.0<\hat{\tau}$	12.6	0	1.5	3
Hydrodynamic Models	ν(10^{-4} m^2/s)				
1. Constant ν, no slip	4		- .4	11.2	26
	8		- .1	6.2	13
	16		.1	3.2	7
2. Linear ν, $\nu_b = 10^{-1}\nu_s$, no slip	8		- .2	15.3	31
	16		.1	8.7	16
	32		.2	4.5	8
	48		.3	3.0	5
3. Constant ν, $\tau_s = \tau_0$ slip with $c_D = .01$	8		0	9.7	19
	16		.2	6.0	11
	32		.3	3.5	6
	48		.4	2.5	2
Same but $\overline{\tau}_s = \tau_0/2$	16		.2	6.6	12

Table 2 Current speeds 1 m above the bottom averaged over mooring stations C1-C6 (Fig. 5) for different values of wind mixing or eddy viscosity. Subscripts 0,1,2 refer to hydraulic flow and currents induced by wind stress along and normal to transect, respectively, as in Eq. (24) with $\tau_0 = 10^{-1}$ N/m^2.

Empirical Model	$\hat{\tau}$ (10^{-2} N/m^2)		Current speed (cm/s)			
	Class	Mean	$\lvert v_0 \rvert$	$\lvert v_1 \rvert$	$\lvert v_2 \rvert$	$\frac{\lvert v_1 \rvert + \lvert v_2 \rvert}{2}$
$\hat{\tau}$ = daily rms of wind stress	$\hat{\tau} < 4.5$	2.8	4.6	7.5	6.3	6.9
	$4.5 < \hat{\tau} < 9.0$	6.1	4.8	4.9	3.6	4.2
	$9.0 < \hat{\tau}$	12.6	4.6	2.0	2.4	2.2
Hydrodynamic Models	ν(10^{-4} m^2/s)					
1. Constant ν, no slip	4		2.6	8.9	7.4	8.1
	8		2.4	4.8	4.0	4.4
	16		2.2	2.4	2.1	2.2
2. Linear ν, $\nu_b = \nu_s/10$, no slip	8		3.7	12.9	12.2	12.5
	16		3.4	7.1	6.8	6.9
	32		3.2	3.7	3.5	3.6
	48		3.2	2.5	2.3	2.4
3. Constant ν, $\tau_s = \tau_0$ slip with $c_D = .01$	8		3.8	7.6	7.2	7.4
	16		4.0	5.0	5.2	5.1
	32		4.1	3.4	4.1	3.7
	48		4.3	2.9	3.7	3.3
Same but $\tau_s = \tau_0/2$	16		4.0	5.6	6.4	6.0

FIGURE LEGENDS

Figure 1 Bottom stress in pressure-driven currents as a function of pressure gradient (above) and eddy viscosity at the surface (below) for different models discussed in the text.

Figure 2 Velocity ratio (above) and difference of direction (below) between current 1 m above the bottom and vertical-mean current as a function of eddy viscosity at the surface in pressure-driven flow for different models discussed in the text.

Figure 3 Bottom stress in wind-driven flow with zero net transport as a function of wind stress (above) and eddy viscosity at the surface (below) for different models discussed in the text.

Figure 4 Velocity (above) and direction relative to wind direction (below) of current 1 m above the bottom as a function of eddy viscosity at the surface in wind-driven flow with zero net transport for different models discussed in the text.

Figure 5 Location of wind recorders, current meters and shore-based water level gauges in Lake St. Clair, June-November, 1985.

PRESSURE - DRIVEN CURRENT (H = 5m)

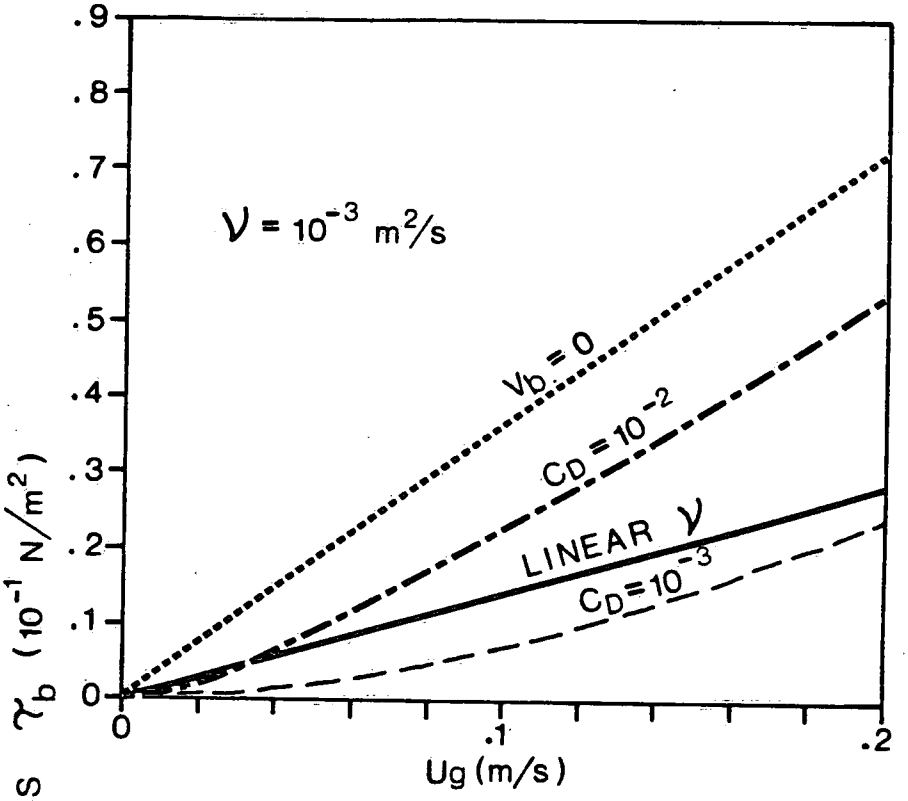

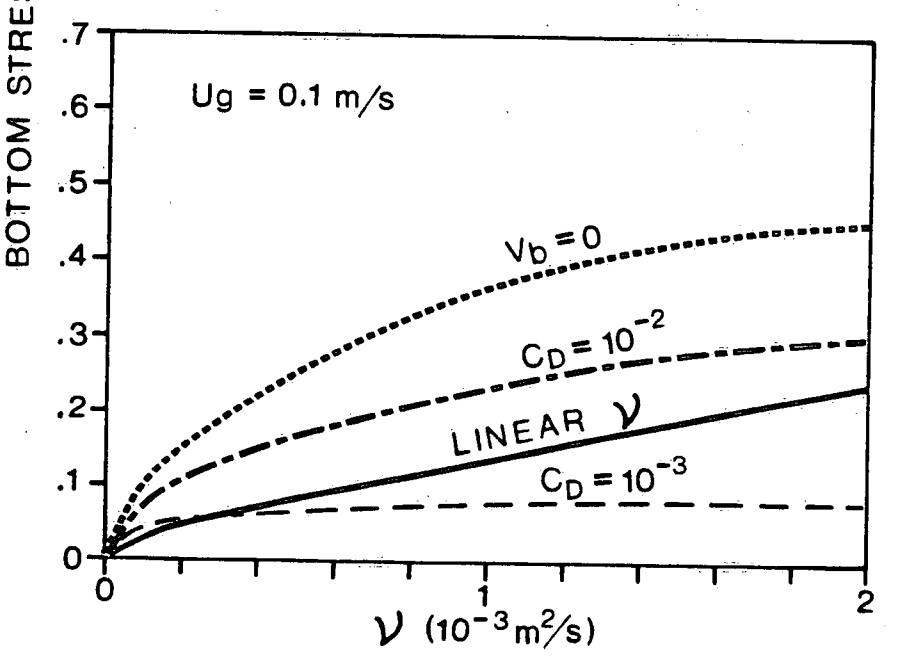

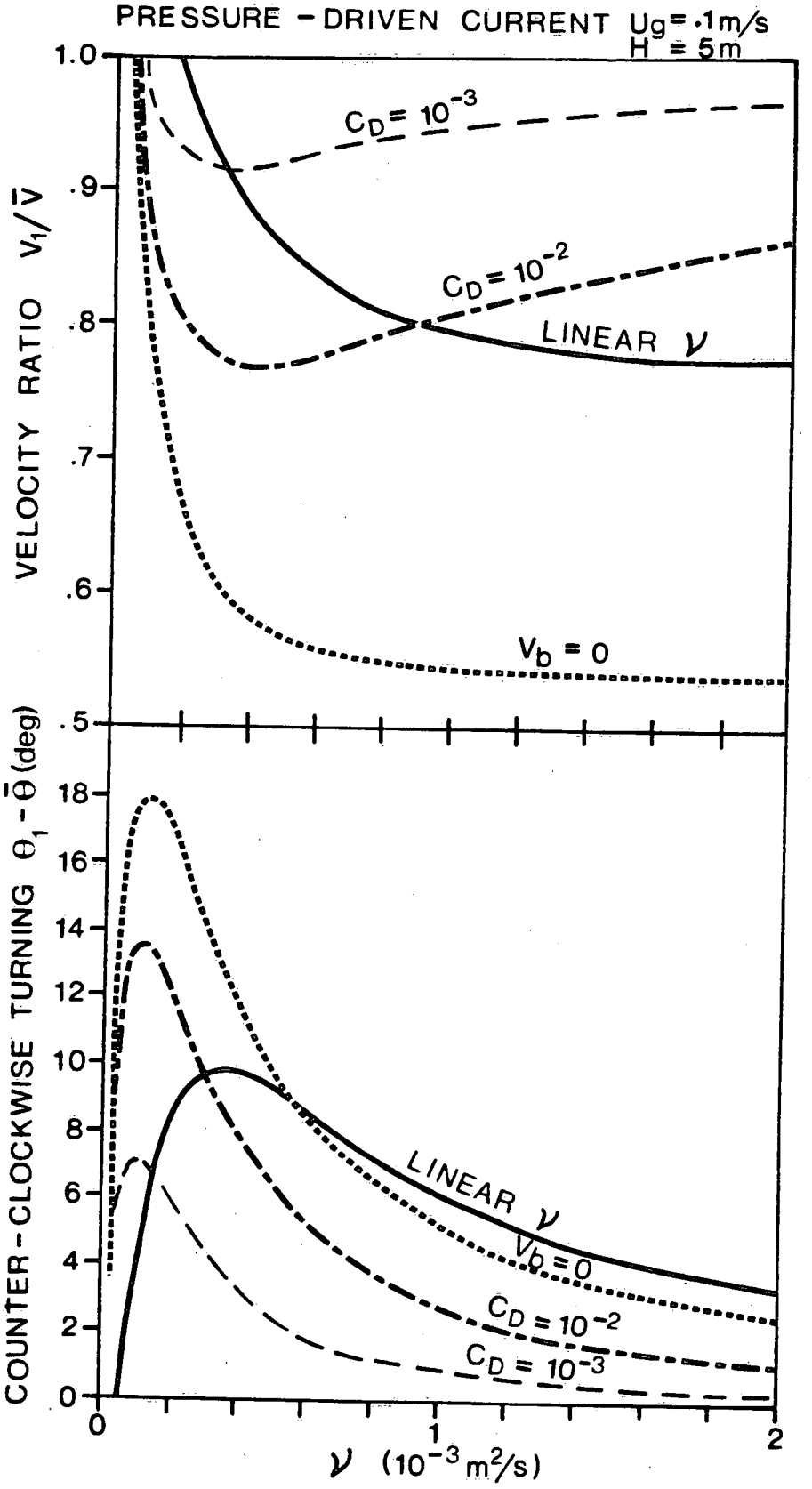
PRESSURE - DRIVEN CURRENT Ug = .1m/s
H = 5m
VELOCITY RATIO $V_1/\bar{V}$
1.0
.9
.8
.7
.6
.5
$C_D = 10^{-3}$
$C_D = 10^{-2}$
LINEAR ν
$V_b = 0$
COUNTER-CLOCKWISE TURNING $\theta_1 - \bar{\theta}$ (deg)
18
16
14
12
10
8
6
4
2
0
LINEAR ν
$V_b = 0$
$C_D = 10^{-2}$
$C_D = 10^{-3}$
0
1
2
ν (10^{-3} m^2/s)

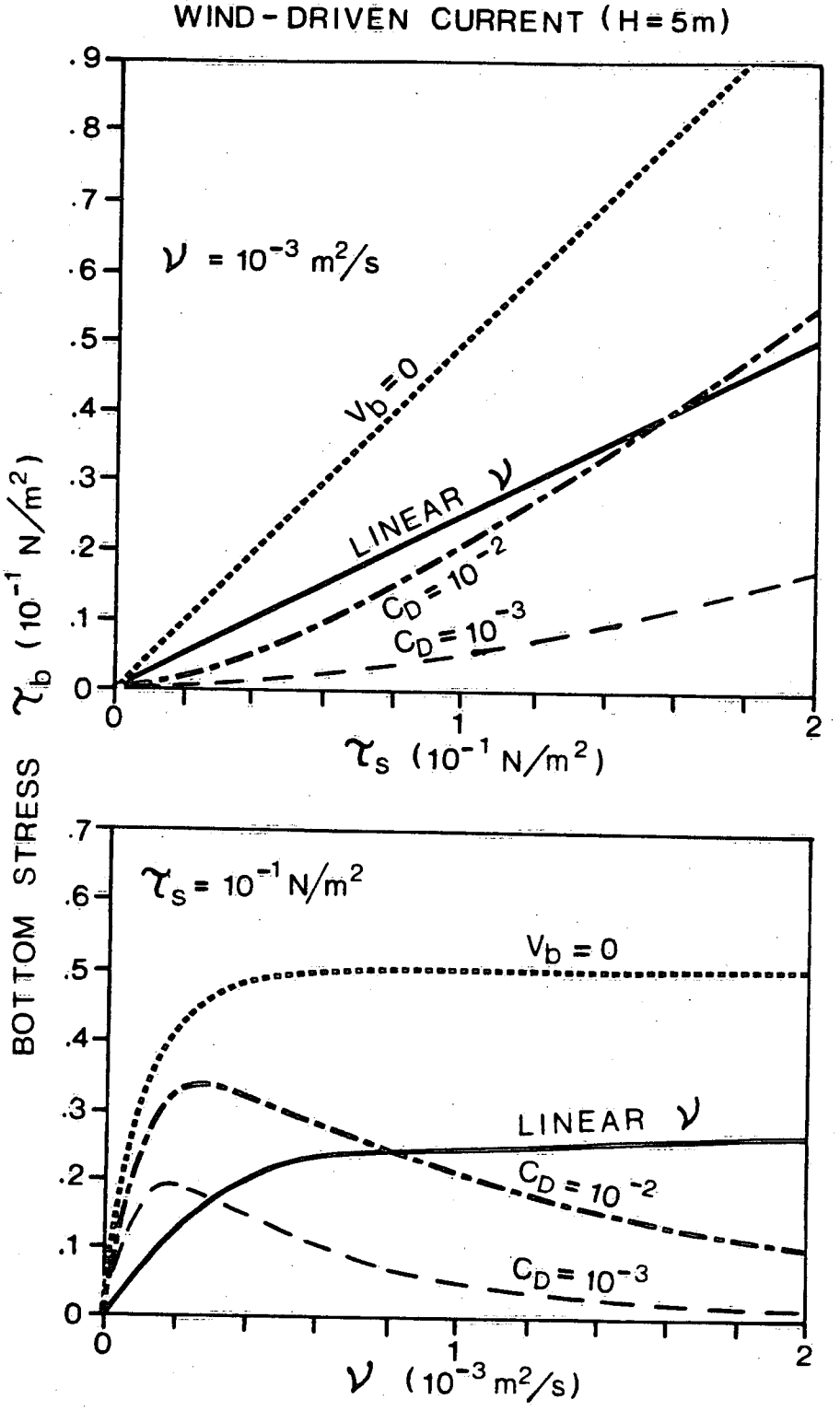
WIND-DRIVEN CURRENT (H=5m)
BOTTOM STRESS
τ_b (10^{-1} N/m^2)
ν = 10^{-3} m^2/s
V_b = 0
LINEAR ν
$C_D = 10^{-2}$
$C_D = 10^{-3}$
τ_s (10^{-1} N/m^2)
τ_s = 10^{-1} N/m^2
V_b = 0
LINEAR ν
$C_D = 10^{-2}$
$C_D = 10^{-3}$
ν (10^{-3} m^2/s)

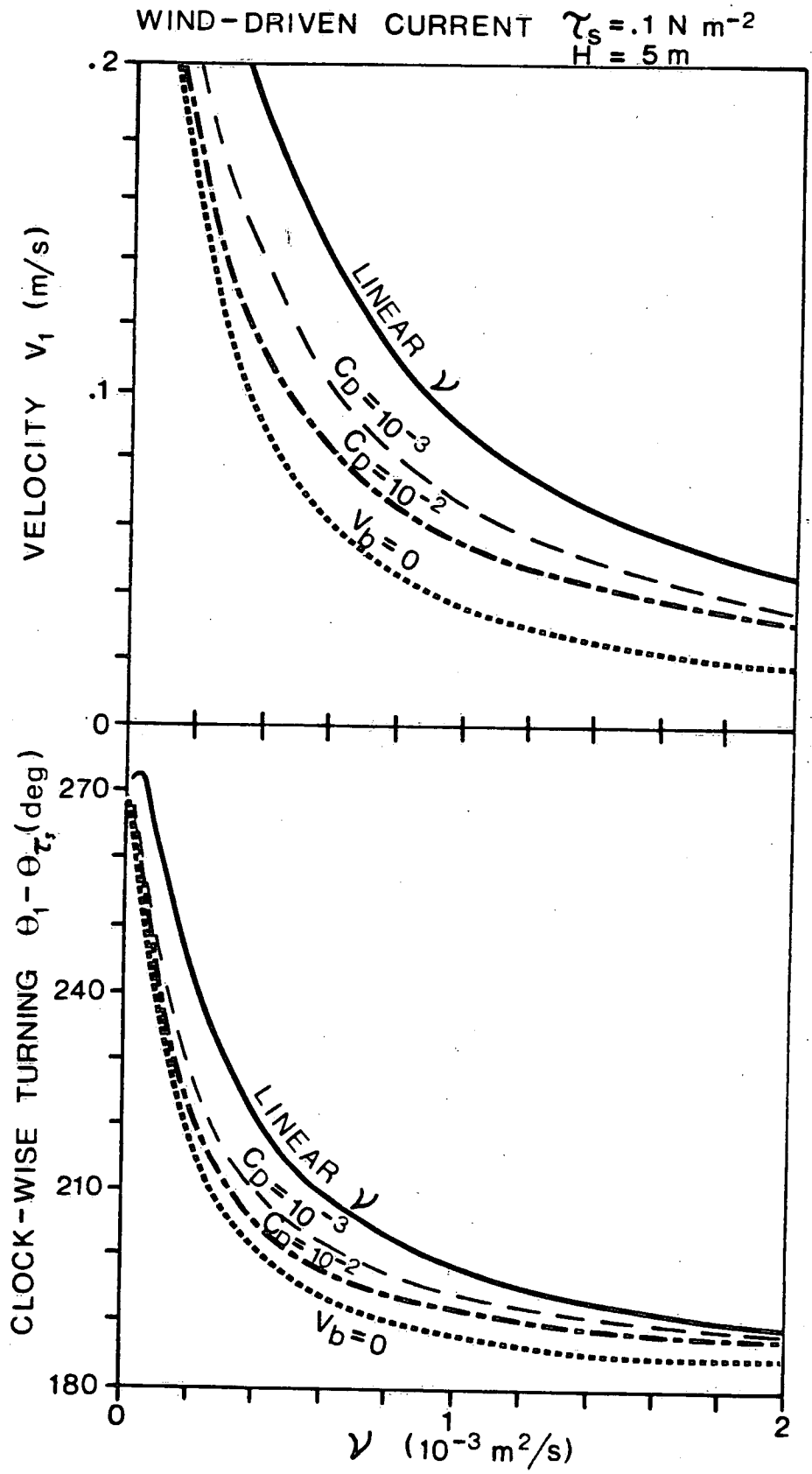
WIND-DRIVEN CURRENT $\tau_s = .1$ N m^{-2}
H = 5 m
VELOCITY V_1 (m/s)
.2
.1
0
LINEAR ν
$C_D = 10^{-3}$
$C_D = 10^{-2}$
$V_b = 0$
CLOCK-WISE TURNING $\theta_1 - \theta_{\tau_s}$ (deg)
270
240
210
180
0
1
2
ν (10^{-3} m^2/s)

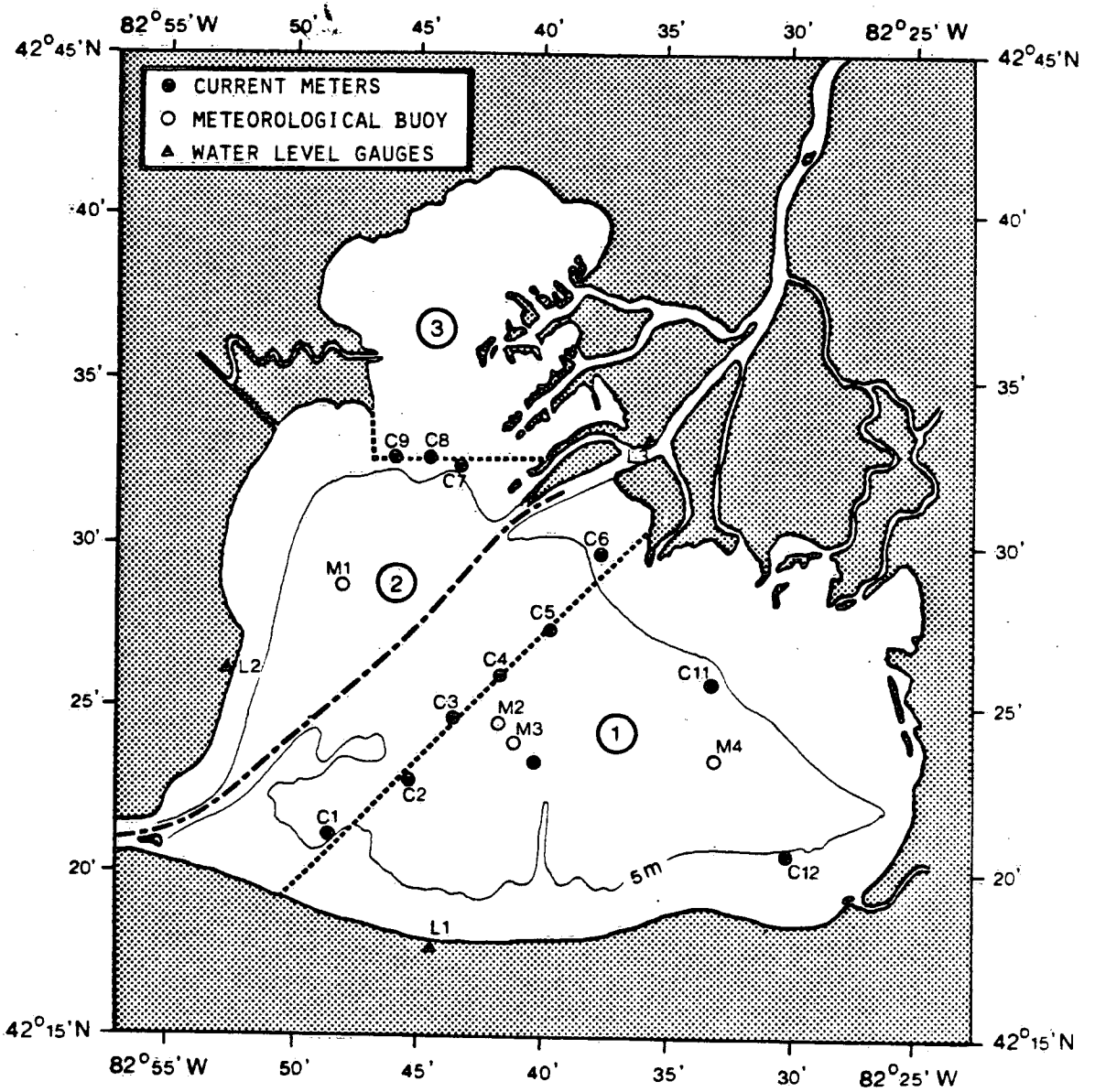
82°55'W
50'
45'
40'
35'
30'
82°25' W
42°45'N
42°15'N
40'
35'
30'
25'
20'
CURRENT METERS
METEOROLOGICAL BUOY
WATER LEVEL GAUGES
3
2
1
C9
C8
C7
C6
C5
C4
C3
C2
C1
C11
C12
M1
M2
M3
M4
L1
L2
L3
5m

APPENDIX

Steady-State Ekman Theory

It will be convenient to introduce the following definitions. First, the characteristic depth of the problem is the "Ekman depth"

$$\Delta \equiv \sqrt{\frac{2\nu}{f}} \tag{3.1}$$

where ν is the kinematic vertical eddy viscosity, assumed to be constant. This depth is proportional to the "depth of frictional influence," as defined in Ekman's original studies, by a factor, π. The nondimensional water depth and vertical coordinate is

$$\delta \equiv \frac{H}{\Delta}, \quad \zeta \equiv \frac{z}{\Delta} \tag{3.2}$$

This nondimensional depth is inversely proportional to the so-called "Ekman number," which is usually defined as Δ^2/H^2 and is a measure of the importance of the vertical friction term in equations of motion. Finally, the geostrophic current

$$u_g = -\frac{1}{\rho f}\frac{\partial p}{\partial y}, \quad v_g = \frac{1}{\rho f}\frac{\partial p}{\partial x} \tag{3.3}$$

which is obviously independent of depth under homogeneous, hydrostatic conditions.

The steady-state equations of motion, under the above conditions, may be written

$$\nu \frac{\partial^2 u}{\partial z^2} + fv = fv_g, \quad \nu \frac{\partial^2 v}{\partial z^2} - fu = -fu_g \tag{3.4}$$

with boundary conditions, assuming no slip at the bottom,

$$\begin{gathered} \nu \frac{\partial u}{\partial z} = \frac{\tau_{xz}}{\rho}, \ \nu \frac{\partial v}{\partial z} = \frac{\tau_{xy}}{\rho} \text{ at } z = 0 \\ u = v = 0 \text{ at } z = -H \end{gathered} \tag{3.5}$$

The solution is most readily obtained by defining the complex velocity, $u + iv$, and the result can be written

$$\begin{aligned} u &= \left(1 - \frac{\alpha}{c}\right) u_g - \frac{\beta}{c} v_g + \frac{1}{\Delta \rho f}\left(\frac{\gamma + \varepsilon}{c}\tau_{xz} + \frac{\gamma - \varepsilon}{c}\tau_{xy}\right) \\ v &= \left(1 - \frac{\alpha}{c}\right) v_g + \frac{\beta}{c} u_g + \frac{1}{\Delta \rho f}\left(\frac{\gamma + \varepsilon}{c}\tau_{xy} - \frac{\gamma - \varepsilon}{c}\tau_{xz}\right) \end{aligned} \tag{3.6}$$

where c is a nondimensional constant defined by

$$c \equiv \cosh(2\delta) + \cos(2\delta) \tag{3.7}$$

and α, β, γ, ε are nondimensional functions of the vertical coordinate given by

$$\begin{aligned} \alpha(z) &\equiv \cosh(\delta+\zeta)\cos(\delta-\zeta) + \cosh(\delta-\zeta)\cos(\delta+\zeta) \\ \beta(z) &\equiv \sinh(\delta+\zeta)\sin(\delta-\zeta) + \sinh(\delta-\zeta)\sin(\delta+\zeta) \\ \gamma(z) &\equiv \sinh(2\delta+\zeta)\cos(\zeta) + \sinh(\zeta)\cos(2\delta+\zeta) \\ \varepsilon(z) &\equiv \cosh(2\delta+\zeta)\sin(\zeta) + \cosh(\zeta)\sin(2\delta+\zeta) \end{aligned} \tag{3.8}$$

The vertically integrated transport is most easily obtained by determining first the vertical derivative of the velocity at the bottom, i.e. the bottom stress, and then using the vertically integrated forms of the equations of motion (3.4).

$$U \equiv \int_{-H}^{0} u\,dz = H\left[(1-B)u_w - Av_w\right] + \frac{1}{\rho f}\left[E\tau_{sx} + (1-F)\tau_{sw}\right]$$
$$V \equiv \int_{-H}^{0} v\,dz = H\left[(1-B)v_w + Au_w\right] + \frac{1}{\rho f}\left[E\tau_{sw} - (1-F)\tau_{sx}\right] \tag{3.10}$$

where A, B, E, and F are nondimensional constants defined by

$$A \equiv \frac{\sinh(2\delta) - \sin(2\delta)}{2\delta c}, \quad B \equiv \frac{\sinh(2\delta) + \sin(2\delta)}{2\delta c}$$
$$E \equiv \frac{2\sinh(\delta)\sin(\delta)}{c}, \quad F \equiv \frac{2\cosh(\delta)\cos(\delta)}{c} \tag{3.11}$$

Thus, from (3.3) and (3.10)

$$\frac{\partial p}{\partial x} = \rho f(PV - QU) + R\tau_{sx} + S\tau_{sw}$$
$$\frac{\partial p}{\partial y} = -\rho f(PU + QV) + R\tau_{sw} - S\tau_{sx} \tag{5.14}$$

where the depth-dependent coefficients are defined

$$Q \equiv \frac{A}{GH}, \; P \equiv \frac{1-B}{GH}, \; G \equiv A^2 + (1-B)^2$$
$$R \equiv QE + P(1-F), \quad S \equiv Q(1-F) - PE \tag{5.15}$$

and where the coefficients A, B, E, and F have been defined by (3.11). Then, after cross-differentiation

$$\nabla\cdot(Q\nabla\Psi) - J(P, \Psi) = \text{curl}\left(\frac{R\,\tau_s}{\rho f}\right) - \text{div}\left(\frac{S\,\tau_s}{\rho f}\right) \tag{5.16}$$

The dependence of these coefficients on nondimensional depth, δ, is illustrated in Fig. 3.1.